

Higher potential compound flood risk in Northern Europe under anthropogenic climate change

E. Bevacqua^{1*}, D. Maraun¹, M. I. Voudoukas^{2,3},
E. Voukouvalas², M. Vrac⁴, L. Mentaschi², and M. Widmann⁵

March 21, 2018

1. Wegener Center for Climate and Global Change, University of Graz, Graz, Austria.
2. European Commission, Joint European Research Centre (JRC), Ispra, Italy.
3. Department of Marine Sciences, University of the Aegean, Mitilene, Greece.
4. Laboratoire des Sciences du Climat et de l'Environnement, CNRS/IPSL, Gif-sur-Yvette, France.
5. School of Geography, Earth and Environmental Sciences, University of Birmingham, Birmingham, UK.

*e-mail: emanuele.bevacqua@uni-graz.at

Compound flooding (CF) is an extreme event taking place in low-lying coastal areas as a result of co-occurring high sea level and large amounts of runoff, caused by precipitation. The impact from the two hazards occurring individually can be significantly lower than the result of their interaction^{1,2,3,4}. Both the risk of storm surges and heavy precipitation, as well as their interplay is likely to change in response to anthropogenic global warming. Despite their relevance, a comprehensive risk assessment beyond individual locations at the country scale is missing. In particular, no studies have examined possible future CF risk. Here we estimate the potential CF risk along the European coasts both for present and future climate according to the business-as-usual (RCP8.5) scenario. Under current climate conditions, the locations experiencing the highest risk are mostly located along the Mediterranean Sea. However, future climate projections show emerging risk along parts of the Atlantic coast and the North Sea. The increase of the risk is mostly driven by an intensification of precipitation extremes. In several European regions, increasing CF risk should be considered as a potential hazard aggravating the risk caused by mean sea level rise (SLR).

CF is a coastal hazard and may cause damages and fatalities. Prominent examples from Europe are the Thames flood in London, 1928; the flash flood in Lisbon, 1967⁵; the Avon flood in Bristol, 2014; and the Ravenna flood in 2015⁴. In 2012, the Netherlands almost experienced a flooding of the water board Noorderzijlvest, which led to precautionary evacuation^{6,7}. The recently released pan-European (though not fully comprehensive) HANZE database⁸ lists 24 co-occurrences of storm surges and river floods along the Irish, UK, Belgian and Polish coasts, the French Atlantic and Mediterranean coast, and the Italian Adriatic coast. The risk of CF is in particular increased if storm surge and river flood do not occur independently. Ignoring this dependence may substantially underestimate the resulting risk^{4,3,6,9,10}.

Co-occurring storm surge and heavy rainfall are driven by deep low pressure systems³. Whereas precipitation extremes alone can be caused by convection without intense cyclonic activity¹¹, the latter is a precondition for extreme surges (Fig. 1). Intense cyclones drive storm surges through strong winds pushing water towards the coast, and the barometric pressure effect^{12,4}. CF can be caused by several mechanisms³. A storm surge can block or slow down the precipitation drainage into the sea⁴, causing flooding along the coast^{3,6}. Runoff from a river may require a certain time to drain into the sea such that precipitation may have to occur well before the storm surge. Similarly, flood levels of a storm surge may be amplified by any significant amount of precipitation³. Finally, a flood may occur when precipitation falls on wet soil that is saturated by a preceding storm surge. The relative importance of these mechanisms in a particular location depends both on the local climate and topography³.

Several studies have demonstrated the importance and damaging nature of CF for selected locations^{6,7,4,13}. Comprehensive studies, however, exist only for the UK¹², Australia¹⁴ and the US coast³. The latter study detected an increasing risk of CF during the past decades, although it was not possible to attribute the changing risk to anthropogenic climate change. But given that extreme precipitation¹⁵, river flooding¹⁶, and extreme sea levels^{17,18,19} are expected to increase under future climate change, it is likely that also the risk of CF will increase along with these driving processes. Yet even though coastal cities are expected to further grow in the coming decades¹⁹ and more and more people will be exposed to CF, no studies have investigated future CF risk.

Our study aims to close this research gap. We analyse present and future potential CF risk along the European coastlines. A precise CF risk assessment can in practice only be site-specific because the actual risk depends strongly on local conditions such as the shape of the coastline, the orography and land surface of the surrounding land area where precipitation is collected, the existing flood protection, and the exposed population and assets. Modelling such local detail would, however, preclude a continental scale analysis. Thus we limit ourselves to modelling *potential CF risk*: we follow the approach of previous studies^{18,3} and model the probability of a co-occurrence of extreme sea levels and heavy precipitation. For the sake of brevity, however, we will write of CF risk only. At the end of the 21st century, SLR will be the primary threat for

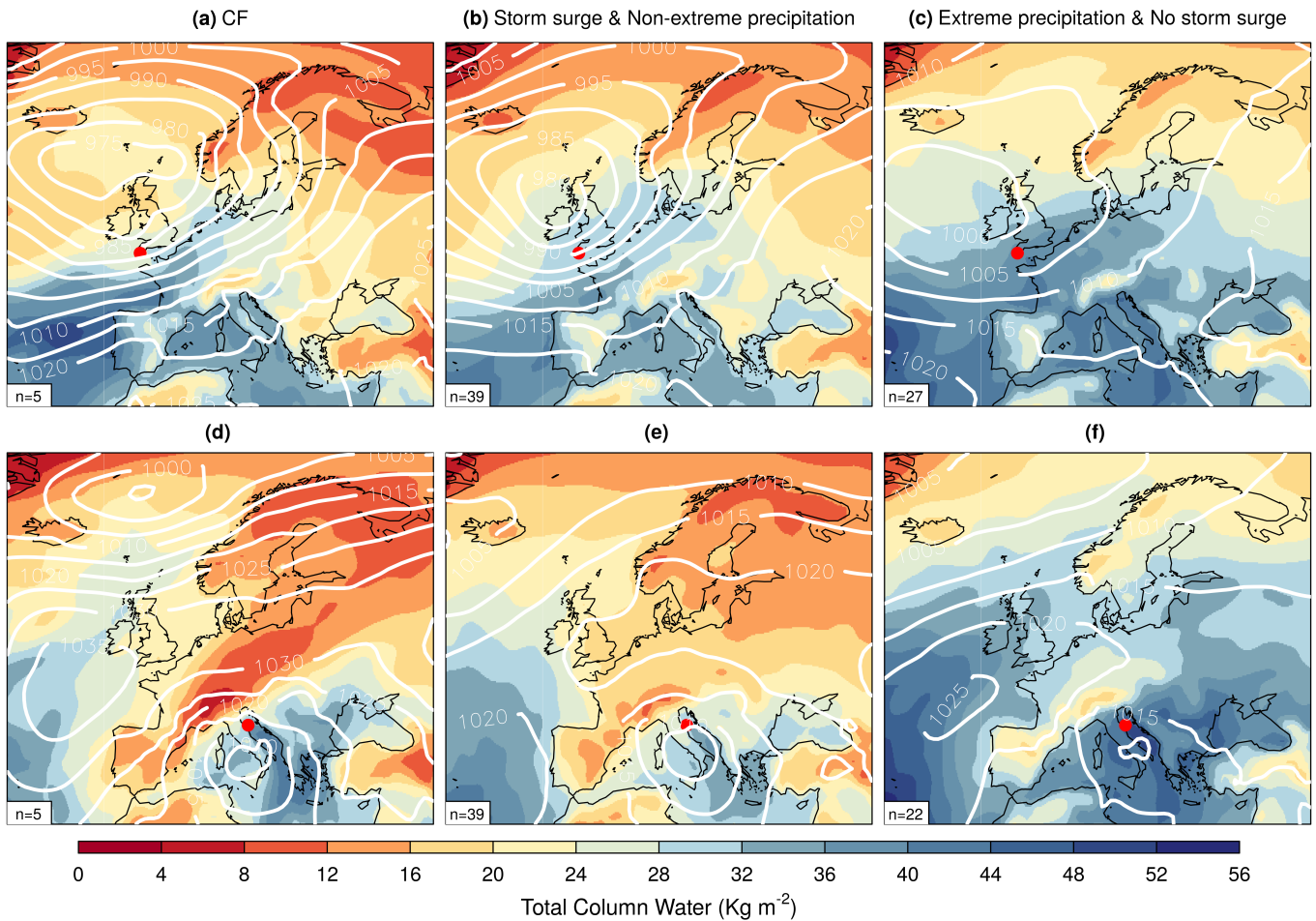


Figure 1: Synoptic weather conditions driving extreme events. Composite maps of sea level pressure (hPa, in white) and total column water fields computed over days where extreme events ($> 99.5^{th}$ percentile) occurred in Plymouth (UK, top) and Ancona (Italy, bottom) indicated by the red dots (based on ERA-Interim data, 1980-2014). Here, the astronomical tide component of the sea level is not considered to focus only on the meteorological driven part. Extreme events type: **(a,d)** compound flooding (CF), **(b,e)** storm surge but not extreme precipitation, **(c,f)** extreme precipitation but not storm surge. The total number of extreme events considered for computing the composite maps is shown at the bottom-left corner of the panels. Storm surges include the wave setup contribution (see text).

55 coastal areas (Supplementary Fig. S1). We assume that societies will adapt to this impact of climate change by raising dikes,
 56 constructing new flood protection, or abandoning coastal areas^{18,19}. For the projections we therefore assess the additional
 57 CF risk, without considering mean SLR, which also allows us to focus more on the meteorologically-driven CF.

58 To characterise extreme sea level, we consider daily maximum values of the superposition of surges (including waves)
 59 and astronomical tides. In the following, we will refer to these maxima simply as sea level. Storm surges and waves
 60 are simulated with the hydrodynamic DFLOW FM^{20,21,17,22} and Wavewatch III^{23,17,22} models respectively, driven with

61 ERA-Interim reanalysis data²⁴ for present climate (1970-2004) and with six selected CMIP5 models²⁵ for future climate
62 (2070-2099). Precipitation is directly taken from the reanalysis and the climate models. On each day, we consider accumu-
63 lated precipitation within a time range of ± 1 days, which allows us to account for the mentioned mechanisms responsible
64 for CF, and precipitation occurring just before and after midnight of the storm surge day²⁶. We define univariate extremes
65 of the individual hazards as events occurring on average every 200 days for sea level, and every 200 wet days for precipi-
66 tation respectively. CF return periods are defined as the average waiting time between the co-occurrence of these extreme
67 events^{27,28,29} (Supplementary Fig. S4). We model the dependence of sea level and precipitation extremes by a copula-based
68 multivariate probability model. For details refer to the Methods section, and for an evaluation of the simulated CF risk see
69 the supplementary information (Supplementary Fig. S2, S3 and S5).

70 The highest CF risk in present climate is experienced mostly along the Mediterranean Sea (Fig. 2a). The Atlantic coast
71 appears to be particularly exposed to co-occurring storm surges and extreme precipitation (Fig. 2b). But here the effective
72 risk is slightly reduced because of the high tidal range (compare Fig. 2a and 2b): no CF occurs when the peak of the storm
73 surge occurs during low astronomical tide³⁰. The Gulf of Valencia (Spain), the Gulf of Lion (France), south- and north-
74 eastern Italy, the northwest Aegean coast, southern Turkey, the Levante region and the Eastern black sea coast are among
75 the upper $\sim 2\%$ most prone to CF with return periods of less than four years (Fig. 2a). The statistical dependence between
76 sea level and precipitation greatly enhances the risk of CF along the European coasts: the CF return period increases by up to
77 two orders of magnitude when ignoring the dependence (Fig. 2c).

78 In a warmer future climate, the risk of CF is projected to robustly increase particularly along the coast of Ireland, the west
79 coast of Great Britain, northern France, the east coast of the North Sea, Italy and the eastern half of the Black Sea (Fig. 3a,
80 Supplementary Fig. S6). Hotspot regions of emerging compound risk where return periods will decrease to less than 4 years
81 are the Bristol Channel and the Devon and Cornwall coast in the UK, the Frisian coast of the Netherlands and Germany (Fig.
82 3b). The forced climate change signal appears to emerge from the uncertainty about present risk mostly along the Western
83 British Isles, the North and Baltic Sea (regions 3, 4, and 5 in Fig. 3c). Along the Noorderzijlvest water board, which also
84 faces the greatest SLR, the probability of potential CF occurrence will double. The Norwegian West coast around Bergen
85 will see a fourfold increase in potential CF frequency. Along much of the Mediterranean coast, climate models do not agree
86 about the direction of future changes in CF risk, along the Strait of Gibraltar CF risk is even expected to decrease (Fig. 3a,
87 Supplementary Fig. S6).

88 Changes in CF risk can in principle be caused by changes in the risk of extreme sea levels, in the risk of extreme
89 precipitation, or in the dependence between both hazards^{6,3,4,9}. For Europe and the Mediterranean, the main driver of future
90 changes in CF risk appears to be changes in precipitation (Fig. 4). Changes in risk due to changes in the dependence between
91 precipitation and extreme sea levels are minor (panel a, see also Methods), and can only explain the overall decrease in CF

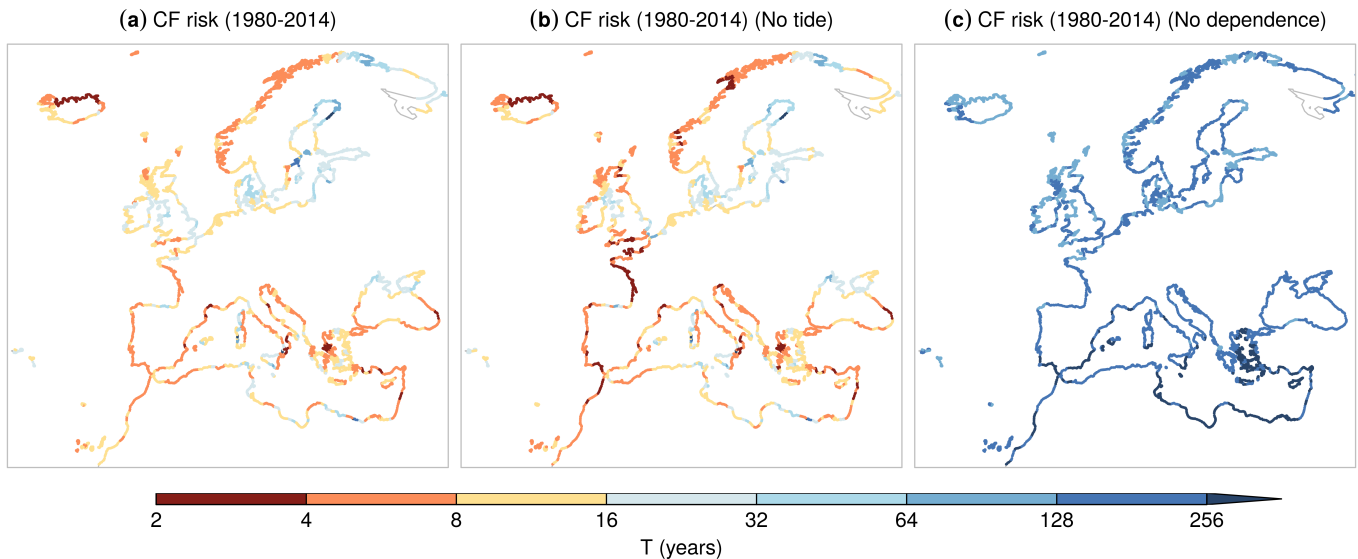


Figure 2: **Present potential compound flood (CF) risk.** Return periods of CF (co-occurring sea level and precipitation extremes, i.e. $> 99.5^{th}$ percentiles) based on ERA-Interim data. In panel (a), sea level includes surge and astronomical tides. To isolate the effect of tides on the resulting potential CF risk, panel (b) shows sea level without including astronomical tides. In panel (c), sea level and precipitation are assumed to be independent.

92 risk along the West African coast. Also changes in risk related to extreme sea levels (panel b, also Supplementary Fig. S7 and
 93 S6). A warmer atmosphere will allow storms to carry more moisture resulting in heavier precipitation. This thermodynamic
 94 effect dominates along the North Atlantic storm track in Northern Europe, and the Mediterranean storm track¹⁵. But weaker
 95 upward winds will reduce or balance the thermodynamic increases of extreme precipitation along the North African coast,
 96 and will even reverse the full precipitation response over north-western Africa¹⁵ (panel c, also Supplementary Fig. S7).

97 In a future climate, sea level rise will be the primary threat along coastal areas, and societies will likely adapt to this
 98 risk^{18,19}. Here we have shown that CF may pose a severe additional hazard that has to be taken into account for a full risk
 99 assessment. In particular Northern Europe will experience an increased risk of CF. There it is key to consider increasing
 100 precipitation intensities when planning adaptation measures against coastal flooding. The overall risk of CF is strongly
 101 aggravated by the dependence between surges and precipitation.

102 To enable a continental scale assessment, we have considered potential flood risk without accounting for the individual
 103 local conditions. Users interested in CF risk at a specific site will know their local setting and should put our findings
 104 into perspective accordingly. If the particular site is not prone to surges and fluvial or pluvial flooding, the real CF may be
 105 negligible even where we identified a high potential risk. In locations, where surges and pluvial flooding are real hazards, our
 106 study will provide an initial guess of future changes in CF risk. As a basis for local adaptation planning, a full site-specific
 107 understanding of CF is necessary. To this end, a complex modelling chain is required³ which can simultaneously integrate

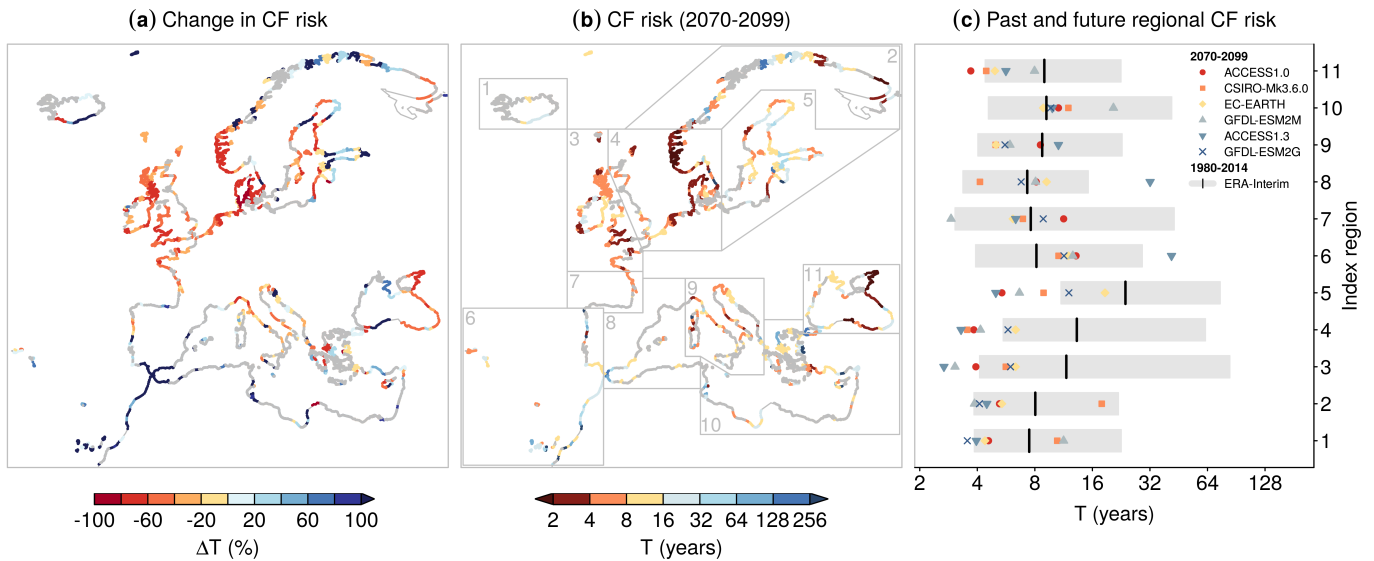


Figure 3: **Future potential compound flood (CF) risk.** (a) Multi-model mean of projected change (%) of CF return periods, between future (2070-2099) and present (1970-2004) climate. (b) Return periods for the future (2070-2099). Grey points indicate locations where less than 80% of the models (five out of six) agree on the sign of the risk change (four out of five models in the Black Sea). Grey points in (a) and (b) are slightly different, as the former are computed taking into account the past period (1970-2004) and the latter the period (1980-2004) (see delta change approach in Methods). (c) Median value of CF return periods over regions defined in (b) for past (1980-2014, based on ERA-Interim (Fig. 2a)) and future (2070-2099) climate, separately for individual models. For ERA-Interim, grey shading illustrates the sampling uncertainty 95% range.

108 information about precipitation, discharge, surges, topography and land-use, relative sea level rise and available or planned
 109 flood protections.

110 Methods

111 **Data.** Storm surges were simulated with the DFLOW FM model using a flexible mesh setup (forced with 6-hourly wind
 112 and atmospheric pressure fields)^{22,17,20,21}. Waves were simulated with the model Wavewatch III^{22,23,17} (forced with 6-hourly
 113 wind field). Astronomical tides were simulated every six hours using the FES2012 model^{31,32,20}, which makes use of satellite
 114 altimetry data. The resulting sea level data are available every ~ 25 km along the coastline. Comprehensive validation and
 115 detailed information of the models can be found in refs.^{17,22,23,20,21}. Our analysis is based on quantile values, therefore we
 116 do not bias correct simulated data. Sea level and precipitation data are based on ERA-Interim and six selected models from
 117 the CMIP5 multi-model ensemble (Supplementary Table 1). Precipitation was taken from the grid point nearest to each
 118 coastal location. CMIP5 models were selected based on the skill in representing the synoptic climatologies and inter-annual

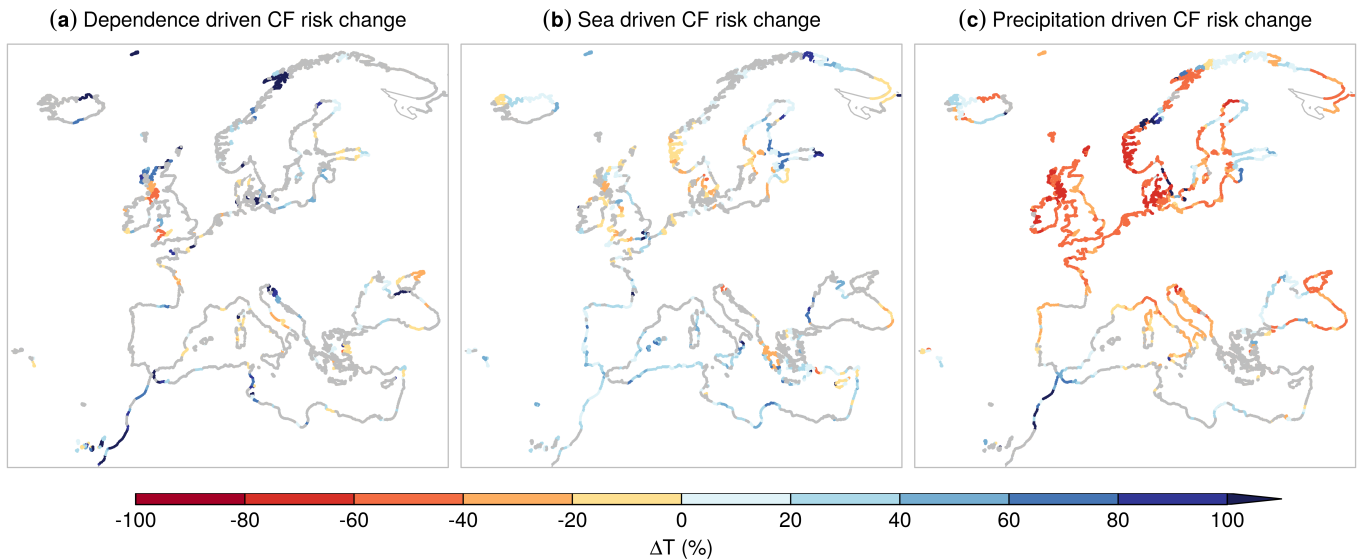


Figure 4: **Attribution of potential compound flood (CF) risk change to changes in dependence and marginal distribution.** Multi-model mean of projected change (%) of CF return periods between future (2070-2099) and present (1970-2004) when only taking into account future changes of: the overall (a) dependence (Spearman and tail dependence⁴) between sea level and precipitation, (b) sea level distribution, and (c) precipitation distribution (Methods). The total projected risk variation (Fig. 3a) is not given by the sum of these three cases (a, b, c), as the overall dependencies and marginal distributions do not contribute linearly to the CF return periods. SLR is not considered in the definition of future sea levels (see text). Grey points indicate locations where less than 80% of the models (five out of six) agree on the sign of the risk change (four out of five models in the Black Sea).

119 variations across the north-east Atlantic region^{33,23,21,17,22}. The GFDL-ESM2G model was not considered along the Black
 120 Sea coast because of instabilities of the surge model. Choosing well performing CMIP5 models reduces the risk of artefacts
 121 caused by the delta change approach³⁴ (see below).

122 To account for the effect of SLR on the astronomical tide, future astronomical tide amplitudes were re-scaled based on
 123 three land-ice scenarios of water contributions from ice sheets and glaciers¹⁸. Since the sensitivity of the final tide amplitude
 124 to the land-ice scenarios is very small¹⁷, we considered the median of the three scenarios only. The actual observed time-lag
 125 between the surge and astronomical tide sequences is random. The estimated CF return periods are thus just one random
 126 realisation of all possible time-lags between surges and astronomical tides. The most likely CF return period is thus the
 127 median of all possible estimates. For the ERA-Interim driven data, we obtained this estimate by calculating 240 individual
 128 estimates based on the superposition of (i) the simulated surge time series (including waves), and (ii) the randomly shifted
 129 tide time series. The part of the tide series beyond the length of the surge series was moved to the start date. From this
 130 ensemble we computed the median of the CF return periods (Fig. 2a). It turned out that the difference between the standard

131 estimate and the bootstrap-based estimate was small. As this procedure is computationally expensive, we therefore refrained
 132 from applying it to the CMIP5-based data.

133 **Return periods.** We define the bivariate CF return periods^{27,28,29} as the mean waiting time between events where sea
 134 level and precipitation simultaneously exceed the individual 99.5th percentiles $s_{99.5}$ and $p_{99.5}$, respectively. To allow for a
 135 robust estimation, we apply a parametric copula-based bivariate probability distribution. Applying a parametric model for
 136 the full range of values, one would run the risk of biasing the representation of the extreme tail by the bulk of the bivariate
 137 distribution where most data occur. Therefore we apply the model only to pairs of high values. We select pairs where,
 138 simultaneously, sea level values exceed the individual 95th percentile (s_{sel}), and precipitation values exceed the individual
 139 95th percentile of wet days (p_{sel}). In a few locations with very low wet day probabilities, one might end up with selecting
 140 few pairs only. Here we reduce the selection threshold 0.95 to ensure that at least 20 pairs of values are selected (never
 141 below 0.9). Clusters of selected event pairs separated by less than three days are replaced by a unique event which assumes
 142 the maximum sea level S and precipitation P observed in the cluster (see Supplementary Fig. S8).

143 The bivariate return period is thus given as

$$\begin{aligned}
 T(s_{99.5}, p_{99.5}) &= \frac{\mu}{P((s > s_{99.5} \text{ and } p > p_{99.5}) \mid (s > s_{sel} \text{ and } p > p_{sel}))} = \\
 &= \frac{\mu}{1 - u_{s99.5} - u_{p99.5} + C_{SP}(u_{s99.5}, u_{p99.5})}
 \end{aligned}
 \tag{1}$$

144 where μ is the average time elapsing between the selected pairs, $u_{s99.5} = F_S(s_{99.5})$, F_S is the marginal cumulative distribution
 145 of the excesses over the selection threshold (accordingly for precipitation), and C_{SP} is the copula modelling the dependence
 146 between the selected pairs.
 147

148 The marginal distributions of sea level and precipitation beyond the selection thresholds are modelled by a Generalised
 149 Pareto Distribution (GPD). Copulas were fitted to (u_S, u_P) (obtained via empirical marginal cumulative distribution function
 150 (CDF)²⁷), and selected via Akaike information criterion from the families: Gaussian, t, Clayton, Gumbel, Frank, Joe,
 151 BB1, BB6, BB7, BB8. Marginal distributions and copulas were fitted through a maximum likelihood estimator (via the
 152 *ismev*³⁵ and *VineCopula*³⁶ R-packages). Goodness of fit of marginals and copulas was tested based on the Cramer-von-
 153 Mises criterion³⁷ (one-tailed; $N_{boot} = 100$ for copulas) (via the *eva*³⁸ and *VineCopula*³⁶ R-packages respectively). The
 154 projected change (%) of the return period T (Fig. 3a) is estimated as $\Delta T(\%) = 100 \cdot (T^{2070-2099} - T^{1970-2004}) / T^{1970-2004}$ for
 155 the individual CMIP5 models.

156 **Sampling uncertainty of ERA-Interim based CF return periods.** To obtain the 95% sampling uncertainty range of
 157 the ERA-Interim based CF return periods, we apply a resampling procedure (for eleven representative locations where the
 158 median regional return periods are found; see Fig. 3c). We base our estimate of sampling uncertainty on the previously

159 generated 240 bivariate sea level/precipitation time series (where surge and precipitation is identical, only astronomical tides
160 have been resampled). Each of these 240 bivariate time series are used for a further resampling procedure by combining
161 bootstrapped numerator and denominator values of the return period expression (equation (1)). The numerator bootstrapped
162 μ values are obtained based on resampling of the observed times elapsing between the selected pairs (s_i, p_i) employed
163 for fitting the parametric probability density function (pdf); the denominator bootstrapped values are obtained based on
164 resampling of the observed pairs (s_i, p_i) used for the fit of the pdf. The final return period sampling uncertainty range is
165 defined as the 2.5th - 97.5th percentile interval of the 240·240 return period estimates. This procedure is preferred to a
166 classic resampling of all of the pairs, which - here - would overestimate the obtained median return period due to the serial
167 correlation of the sea level time series. Based on a large sample of data without any serial correlation, we estimated that
168 our procedure overestimates by 30% the 95% sampling uncertainty range (with respect to a classic resampling procedure).
169 Thus, conclusions about the detection of a climate change signal in the future (Fig. 3c) are conservative.

170 **Delta change approach.** We computed CF return period for future via the delta change approach³⁹, i.e. multiply-
171 ing the ERA-Interim based historical return period $T_{Era}^{1980-2004}$ by the individual CMIP5 model i variation of the risk
172 $T_{Model\ i}^{2070-2099} / T_{Model\ i}^{1980-2004}$. The present day reference period is the intersection of the ERA-Interim and the historical CMIP5
173 data, for which sea level simulations are available. See Supplementary: (Fig. S5) for comparing return periods based on
174 ERA-Interim and individual CMIP5 models, and (Fig. S9) for CMIP5 model-mean return periods in present and future.

175 **Return period for independent drivers.** We estimated the CF return period assuming independence between precipita-
176 tion and sea level via shuffling (500 times) the cumulated precipitation time series (during 1980-2014), and plugging an
177 independent copula in equation (1). Then, we extracted the median of the 500 return periods associated with the shuffled
178 time series.

179 **Attribution of return period variation.** We carried out three experiments⁴ to assess how the CF risk would change
180 in future when only considering variation - with respect to the present - of: (a) the dependence between sea level and
181 precipitation, (b) the sea level and (c) precipitation overall marginal distributions (i.e. the distribution of the sea level
182 without reference to precipitation, and vice versa). We estimated the relative change of the risk that would have occurred for
183 experiment (i) as $\Delta_{exp\ i} = 100 \cdot (T_{exp\ i}^{fut} - T^{pres}) / T^{pres}$ (Fig. 4), where T^{pres} is the return period for the present period and $T_{exp\ i}^{fut}$ is
184 computed as follows. Experiment (a): given the variables (S_{fut}, P_{fut}) , we got the associated empirical cumulative distribution
185 $(U_{S_{fut}}, U_{P_{fut}})$. From the variables S_{pres} and P_{pres} we defined the empirical CDFs $F_{S_{pres}}$ and $F_{P_{pres}}$, through which we defined
186 $S_a = F_{S_{pres}}^{-1}(U_{S_{fut}})$ and $P_a = F_{P_{pres}}^{-1}(U_{P_{fut}})$. The variables (S_a, P_a) have the same Spearman correlation and tail dependence⁴
187 as (S_{fut}, P_{fut}) , but marginal distributions as in the present period. We computed the return period $T_{exp\ a}^{fut}$ based on (S_a, P_a) .

188 Experiment (b): given the variable S_{pres} , we got the associated empirical cumulative distribution $U_{S_{\text{pres}}}$. From the variable
189 S_{fut} we defined the empirical CDFs $F_{S_{\text{fut}}}$, through which we defined $S_b = F_{S_{\text{fut}}}^{-1}(U_{S_{\text{pres}}})$. The variables (S_b, P_{pres}) have the same
190 Spearman correlation and tail dependence as during the present, but the marginal distribution of S_b is that of the future. We
191 computed the return period $T_{\text{exp } b}^{\text{fut}}$ based on (S_b, P_{pres}) . Experiment (c): as experiment (b), exchanging precipitation and sea
192 level variables.

193 **Data availability**

194 Precipitation data from CMIP5 models are available from the Earth System Grid Federation (ESGF) Peer-to-Peer sys-
195 tem (<https://esgf-node.llnl.gov/projects/cmip5>). Precipitation data from ERA-Interim are available from the
196 ECMWF Public Datasets web interface (<http://apps.ecmwf.int/datasets>). The model FES2012, used for the as-
197 tronomical tides simulations was produced by Noveltis, Legos and CLS Space Oceanography Division and distributed by
198 Aviso, with support from Cnes (<http://www.aviso.altimetry.fr/>). Sea level data can be found in the LISCOAST data
199 collection (<http://data.jrc.ec.europa.eu/collection/LISCOAST>).

200 **Acknowledgements**

201 We acknowledge the World Climate Research Programs Working Group on Coupled Modelling, which is responsible for
202 CMIP, and we thank the climate modeling groups for producing and making available their model output. For CMIP the U.S.
203 Department of Energys Program for Climate Model Diagnosis and Intercomparison provides coordinating support and led
204 development of software infrastructure in partnership with the Global Organization for Earth System Science Portals. We
205 acknowledge the E-OBS dataset from the EU-FP6 project ENSEMBLES (<http://ensembles-eu.metoffice.com>) and
206 the data providers in the ECA&D project (<http://www.ecad.eu>). E.B. received funding from the Volkswagen Foundations
207 CE:LLO project (Az.: 88468), and M.V. from the "EUPHEME" ERA4CS project.

208 **Author Contributions**

209 E.B. and D.M. had the idea of the study and designed the work. E.B. carried out the data analysis. E.B. wrote the paper with
210 D.M., and with contributions from M.I.V. E.B. performed the astronomical tide simulations, M.I.V. and E.V. performed
211 storm surge runs, and L.M. performed the wave runs. E.V., L.M., and M.I.V. collected the observed sea level data and
212 derived the observed astronomical tides. M.V. gave conceptual inputs during the data analysis. All authors discussed the
213 results and commented on the manuscript.

214 **Competing Financial Interests statement**

215 The authors declare no competing financial interest.

216 References

- 217 [1] Seneviratne, S. I. *et al.* Managing the risks of extreme events and disasters to advance climate change adaptation:
218 Changes in climate extremes and their impacts on the natural physical environment 109–230 (2012). URL <https://doi.org/10.1017/cbo9781139177245.006>.
219
- 220 [2] Leonard, M. *et al.* A compound event framework for understanding extreme impacts. *Wiley Interdisciplinary Reviews:*
221 *Climate Change* **5**, 113–128 (2014).
- 222 [3] Wahl, T., Jain, S., Bender, J., Meyers, S. D. & Luther, M. E. Increasing risk of compound flooding from storm surge
223 and rainfall for major us cities. *Nature Climate Change* **5**, 1093–1097 (2015).
- 224 [4] Bevacqua, E., Maraun, D., Haff, I. H., Widmann, M. & Vrac, M. Multivariate statistical modelling of compound events
225 via pair-copula constructions: analysis of floods in ravenna (italy). *Hydrology and Earth System Sciences* **21**, 2701
226 (2017).
- 227 [5] Trigo, R. M. *et al.* The deadliest storm of the 20th century striking portugal: Flood impacts and atmospheric circulation.
228 *Journal of Hydrology* **541**, 597–610 (2016).
- 229 [6] van den Hurk, B., van Meijgaard, E., de Valk, P., van Heeringen, K.-J. & Gooijer, J. Analysis of a compounding surge
230 and precipitation event in the netherlands. *Environmental Research Letters* **10**, 035001 (2015).
- 231 [7] Hazeleger, W. *et al.* Tales of future weather. *Nature Climate Change* **5**, 107–113 (2015).
- 232 [8] Paprotny, D., Morales-Nápoles, O. & Jonkman, S. N. Hanze: a pan-european database of exposure to natural hazards
233 and damaging historical floods since 1870. *Earth System Science Data Discussions* (2017).
- 234 [9] Moftakhari, H. R., Salvadori, G., AghaKouchak, A., Sanders, B. F. & Matthew, R. A. Compounding effects of sea
235 level rise and fluvial flooding. *Proceedings of the National Academy of Sciences* **114**, 9785–9790 (2017).
- 236 [10] Zscheischler, J. & Seneviratne, S. I. Dependence of drivers affects risks associated with compound events. *Science*
237 *Advances* **3**, e1700263 (2017).
- 238 [11] Pfahl, S. & Wernli, H. Quantifying the relevance of cyclones for precipitation extremes. *Journal of Climate* **25**,
239 6770–6780 (2012).
- 240 [12] Svensson, C. & Jones, D. A. Dependence between sea surge, river flow and precipitation in south and west britain.
241 *Hydrology and Earth System Sciences Discussions* **8**, 973–992 (2004).

- 242 [13] Kumbier, K., Carvalho, R. C., Vafeidis, A. T. & Woodroffe, C. D. Investigating compound flooding in an estuary using
243 hydrodynamic modelling: A case study from the shoalhaven river, australia. *Natural Hazards Earth System Science*
244 *Discussion* .
- 245 [14] Zheng, F., Westra, S. & Sisson, S. A. Quantifying the dependence between extreme rainfall and storm surge in the
246 coastal zone. *Journal of hydrology* **505**, 172–187 (2013).
- 247 [15] Pfahl, S., OGorman, P. & Fischer, E. Understanding the regional pattern of projected future changes in extreme
248 precipitation. *Nature Climate Change* **7**, 423–427 (2017).
- 249 [16] Hirabayashi, Y. *et al.* Global flood risk under climate change. *Nature Climate Change* **3**, 816–821 (2013).
- 250 [17] Vousdoukas, M. I., Mentaschi, L., Voukouvalas, E., Verlaan, M. & Feyen, L. Extreme sea levels on the rise along
251 europe’s coasts. *Earth’s Future* **5**, 304–323 (2017).
- 252 [18] Hinkel, J. *et al.* Coastal flood damage and adaptation costs under 21st century sea-level rise. *Proceedings of the*
253 *National Academy of Sciences* **111**, 3292–3297 (2014).
- 254 [19] Hallegatte, S., Green, C., Nicholls, R. J. & Corfee-Morlot, J. Future flood losses in major coastal cities. *Nature climate*
255 *change* **3**, 802–806 (2013).
- 256 [20] Muis, S., Verlaan, M., Winsemius, H. C., Aerts, J. C. & Ward, P. J. A global reanalysis of storm surges and extreme
257 sea levels. *Nature communications* **7** (2016).
- 258 [21] Vousdoukas, M. I., Voukouvalas, E., Annunziato, A., Giardino, A. & Feyen, L. Projections of extreme storm surge
259 levels along europe. *Climate Dynamics* **47**, 3171–3190 (2016).
- 260 [22] Vousdoukas, M. I. *et al.* Global probabilistic projections of extreme sea levels. *Submitted to Nature Communications*
261 (2018).
- 262 [23] Mentaschi, L., Vousdoukas, M. I., Voukouvalas, E., Dosio, A. & Feyen, L. Global changes of extreme coastal wave
263 energy fluxes triggered by intensified teleconnection patterns. *Geophysical Research Letters* **44**, 2416–2426 (2017).
- 264 [24] Dee, D. P. *et al.* The era-interim reanalysis: Configuration and performance of the data assimilation system. *Quarterly*
265 *Journal of the royal meteorological society* **137**, 553–597 (2011).
- 266 [25] Taylor, K. E., Stouffer, R. J. & Meehl, G. A. An overview of cmip5 and the experiment design. *Bulletin of the American*
267 *Meteorological Society* **93**, 485–498 (2012).

- 268 [26] Martius, O., Pfahl, S. & Chevalier, C. A global quantification of compound precipitation and wind extremes. *Geophys-*
269 *ical Research Letters* **43**, 7709–7717 (2016).
- 270 [27] Vandenberghe, S., Verhoest, N., Onof, C. & De Baets, B. A comparative copula-based bivariate frequency analysis of
271 observed and simulated storm events: A case study on bartlett-lewis modeled rainfall. *Water Resources Research* **47**
272 (2011).
- 273 [28] Gräler, B. *et al.* Multivariate return periods in hydrology: a critical and practical review focusing on synthetic design
274 hydrograph estimation. *Hydrology and Earth System Sciences* **17**, 1281–1296 (2013).
- 275 [29] Salvadori, G., Durante, F., Tomasicchio, G. & D’alessandro, F. Practical guidelines for the multivariate assessment of
276 the structural risk in coastal and off-shore engineering. *Coastal Engineering* **95**, 77–83 (2015).
- 277 [30] Haigh, I. D. *et al.* Spatial and temporal analysis of extreme sea level and storm surge events around the coastline of the
278 uk. *Scientific data* **3**, 160107 (2016).

279 **References of the Methods**

- 280 [31] Carrère, L., Lyard, F., Cancet, M., Guillot, A. & Roblou, L. Fes 2012: a new global tidal model taking advantage of
281 nearly 20 years of altimetry. In *20 Years of Progress in Radar Altimetry*, vol. 710 (2013).
- 282 [32] Stammer, D. *et al.* Accuracy assessment of global barotropic ocean tide models. *Reviews of Geophysics* **52**, 243–282
283 (2014).
- 284 [33] Perez, J., Menendez, M., Mendez, F. J. & Losada, I. J. Evaluating the performance of cmip3 and cmip5 global climate
285 models over the north-east atlantic region. *Climate dynamics* **43**, 2663–2680 (2014).
- 286 [34] Maraun, D. *et al.* Towards process-informed bias correction of climate change simulations. *Nature Climate Change* **7**,
287 764 (2017).
- 288 [35] Heffernan, J., Stephenson, A. & Gilleland, E. Ismev: an introduction to statistical modeling of extreme values. *R*
289 *package version 1.41* (2016). URL <https://CRAN.R-project.org/package=ismev>.
- 290 [36] Schepsmeier, U. *et al.* Vinecopula: Statistical inference of vine copulas. *R package version 2.0.5* (2016).
- 291 [37] Genest, C., Rémillard, B. & Beaudoin, D. Goodness-of-fit tests for copulas: A review and a power study. *Insurance:*
292 *Mathematics and economics* **44**, 199–213 (2009).

- 293 [38] Bader, B. & Yan, J. *eva*: Extreme value analysis with goodness-of-fit testing. *R package version 0.2.4* (2016).
- 294 [39] Maraun, D. & Widmann, M. *Statistical Downscaling and Bias Correction for Climate Research* (Cambridge University
295 Press, 2018).